

1     Visualising Excitations at Buried Heterojunctions  
2                     in Organic Semiconductor Blends

3     *Andreas C. Jakowetz<sup>1</sup>, Marcus L. Böhm<sup>1</sup>, Aditya Sadhanala<sup>1</sup>, Sven Huettner<sup>2</sup>, Akshay Rao<sup>\*1</sup>*  
4                     *and Richard H. Friend<sup>\*1</sup>*

5     <sup>1</sup> Cavendish Laboratory, Department of Physics, University of Cambridge, J J Thomson  
6     Avenue, Cambridge, CB3 0HE, United Kingdom

7     <sup>2</sup> Fakultät für Biologie, Chemie und Geowissenschaften, University Bayreuth,  
8     Universitätsstrasse 30, 95440 Bayreuth, Germany

9  
10    e-mail: [ar525@cam.ac.uk](mailto:ar525@cam.ac.uk), [rhf10@cam.ac.uk](mailto:rhf10@cam.ac.uk)

11  
12  
13    KEYWORDS: Interface, Disorder, Charge Generation, Driving Energy, Ultrafast  
14    Spectroscopy, Transient Absorption, Pump-Push, SAXS, WAXS, PDS, Polymer, Fullerene,  
15    Organic Photovoltaics

16 **Abstract:**

17 Interfaces play a crucial role in semiconductor devices, but in many device architectures they  
18 are nanostructured, disordered, and buried away from the surface of the sample. Conventional  
19 optical, X-ray and photoelectron probes often fail to provide interface-specific information in  
20 such systems. Here we develop an all-optical time-resolved method to probe the local  
21 energetic landscape and electronic dynamics at such interfaces, based on the Stark effect  
22 caused by electron-hole pairs photo-generated across the interface. Using this method, we  
23 found that the electronically active sites at the polymer-fullerene interfaces in model bulk-  
24 heterojunction blends fall within the low-energy tail of the absorption spectrum. This  
25 suggests that these sites are highly ordered compared to the bulk of the polymer film, leading  
26 to large wavefunction delocalisation and low site energies. We also detected a 100fs  
27 migration of holes from higher to lower energy sites, consistent with these charges moving  
28 ballistically into more ordered polymer regions. This ultrafast charge motion may be key to  
29 separating electron-hole pairs into free charges against the Coulomb interaction.

30 Understanding the properties of nanoscale and disordered interfaces presents a critical  
31 scientific challenge, cutting across the areas of condensed-matter physics, materials science,  
32 physical chemistry, and biology. A range of techniques, such as atomic resolution electron  
33 microscopy, photoelectron, and X-ray measurements, has been used to probe the properties of  
34 conventional ‘ordered’ interfaces, such as those in inorganic semiconductor or magnetic  
35 heterostructures.<sup>1</sup> Yet, these techniques have proved extremely challenging to apply directly  
36 to nanoscale and disordered interfaces which are often buried away from the surface of the  
37 sample. This means that conventional optical, photoelectron or X-ray techniques are often  
38 swamped by signal from the ‘bulk’ of the samples and not sensitive to the interface. Interface  
39 specific techniques, such as sum-frequency generation (SFG), require well defined and sharp  
40 interfaces in order to generate signal, which makes them unsuited to the disordered and often  
41 random morphologies of these interfaces.<sup>2</sup>

42  
43 Bulk-heterojunctions (BHJs) between organic semiconductors, which comprise an intermixed  
44 blend of p- and n-type semiconductor<sup>3-8</sup>, provide a model disordered nanoscale interface. The  
45 electronic structure and disorder at and near (<5 nm from) these interfaces controls  
46 wavefunction delocalisation, charge transfer, separation and recombination efficiency and  
47 thus the performance of optoelectronic devices, such as organic photovoltaics (OPVs) and  
48 organic light emitting diodes (OLEDs).<sup>9-11</sup> A tremendous amount of work has been done to  
49 understand the physical and chemical structure of these interfaces.<sup>12,13</sup> Yet, to date no  
50 techniques exist that can report directly on the dynamics of populated electronic states at and  
51 near these buried interfaces.

52  
53 Here, we demonstrate an all-optical method to access information on the electronic properties  
54 of such buried and disordered interfaces and their neighbouring electronic sites, and use it to  
55 study model BHJ OPV polymer-fullerene blends. We utilise an ultrafast pump-push-probe

56 technique which measures the quadratic Stark effect caused by electron-hole pairs generated  
57 across the interface between n- and p-type semiconductors. This “electroabsorption” signal  
58 provides a unique signature of the dynamics of electronic states in the interfacial region,  
59 allowing us to precisely map the local energetic landscape that the charges sample as they  
60 move away from the interface. Very surprisingly, we find firstly that the local bandgap of the  
61 electronically active interfacial sites is strongly redshifted compared to the bulk and secondly,  
62 that charges can move from higher-energy to low-energy regions on sub 100fs timescales,  
63 consistent with ballistic motion of holes.

64

65 As model system we use the polymer donor [N-11'-henicosanyl-2,7-carbazole-alt-5,5-(4',7'-  
66 di-2-thienyl-2',1',3'-benzothiadiazole)] (PCDTBT) which is blended with one of the Phenyl-  
67 C<sub>61</sub>-butyric acid methyl ester derivatives mono-PC<sub>61</sub>BM (mPCBM), bis-PC<sub>61</sub>BM (bPCBM),  
68 and tris-PC<sub>61</sub>BM (tPCBM). Weight ratios between polymer and fullerene are 1:1 across the  
69 set of fullerenes and 4:1, 1:1, and 1:4 for PCDTBT:mPCBM blends. The chemical structure  
70 of the materials can be found in Figure 1 (a). UV-Vis and photoluminescence (PL) spectra for  
71 PCDTBT and mono-PCBM, can be found in Figure S1.1. The internal quantum efficiency of  
72 optimised (1:4) PCDTBT:mPCBM blends is close to 100%<sup>14</sup>. The system has been  
73 previously well characterised optically and structurally.<sup>15-18</sup> For instance several studies have  
74 shown that structurally all blends consist of intermixed regions of fullerene and polymer, the  
75 so-called mixed-phase.<sup>12,13</sup> Intercalation of fullerenes between the amorphous PCDTBT  
76 chains is observed<sup>19-21</sup> and strong similarities to fullerenes intercalating in-between MDMO-  
77 PPV are reported.<sup>19,22</sup> Adding more fullerene leads to complete filling of the intercalated sites  
78 and eventually results in pure fullerene domains, this allows for a controlled comparison of  
79 charge separation and the formation of charge transfer states through the variation of  
80 fullerene content.<sup>23</sup> The addition of side groups to the fullerenes leads to increased disorder  
81 in the packing, as has been discussed previously. This is confirmed by small-/wide-angle X-

82 ray scattering (SAXS/WAXS) spectra of the different materials and compositions, which  
83 showed that mono-adduct fullerenes form the largest aggregates, while adding more side  
84 groups lowers aggregate size (see Section S2). Furthermore, increasing fullerene content  
85 leads to larger aggregate size, which leads to formation of larger networks within the  
86 fullerene domain.<sup>24</sup> Increased disorder in the fullerene phase has been linked to inefficient  
87 charge generation, higher charge recombination and poor device performance.<sup>25</sup> Thus the  
88 wide tunability of the system via the choice and amount of fullerene added made PCDTBT an  
89 ideal system to elucidate the role of structure on electronic dynamics. However, the exact  
90 energetic landscape at the interface and effect of the fullerene phase on the packing of the  
91 polymer and how this influences charge dynamics are difficult to quantify due to lack of  
92 suitable interface specific probes.

93

94 Time-resolved optical pump-probe spectroscopies provide powerful ways to study the  
95 electronic properties of such systems.<sup>26</sup> In these methods, a laser pulse excites the sample,  
96 generating excitations such as charges and excitons. Sometime later, a probe pulse  
97 interrogates the sample and measures the change in absorption (transmission) induced by the  
98 pump pulse. Excited states generated by the pump pulse correlate directly to a lower ground-  
99 state population and will thereby lead to a ground-state bleach (GSB) in absorption. While  
100 initial excitations can contribute to the overall signal with stimulated emission (SE) due to  
101 their singlet character, all excited states have a photo-induced absorption (PIA) feature, the  
102 spectral shape of which depends on the material and the nature of the excited state.  
103 Importantly, pump-probe methods provide information on the specific site/chromophore on  
104 which the excitation is when probed, but not on the surrounding sites. Furthermore, these  
105 techniques do not provide any interface specificity, rather they provide information of  
106 whichever site/chromophore the excitation is located on.

107

108 Turning to the case of interfaces, we find that pump-probe spectroscopy can provide  
109 additional information. As illustrated in Figure 1 (c), when excitons are dissociated at the  
110 interface between p- and n-type semiconductors, they form electron-hole (e-h) pairs which  
111 act as a local electric dipole and induce a quadratic Stark shift on the energy levels of the  
112 surrounding molecules. The Stark shift causes a change in the absorption spectra of the  
113 surrounding molecules, normally leading to a redshift in absorption due to lowering of optical  
114 absorption gap. The difference between the two absorption spectra (with and without electric  
115 field), takes the form of a derivative of the absorption spectra and is conventionally referred  
116 to as electroabsorption (EA).<sup>27</sup> This is illustrated in the cartoon in Figure 1(b). Thus, pump-  
117 probe spectroscopy of interfaces contains a mix of GSB, PIA, SE and EA signals, as  
118 illustrated in the lower panel of Figure 1(c).

119  
120 This EA signal has been used to create powerful pump-probe methods to investigate the  
121 interfaces of inorganic and organic material systems.<sup>11,28-30</sup> Recently, we have demonstrated  
122 that this EA can be tracked as a function of time at BHJ interfaces. As the e-h pair separates  
123 across the interface, the electric field associated with it varies, giving rise to a time-dependent  
124 electric field and hence a time-dependent Stark shift and EA signal. By monitoring the  
125 dynamics of the EA signal it is possible to track the separation of e-h pairs on fs timescales.<sup>11</sup>  
126 Using this method it was shown that for the PCDTBT:PCBM (1:4) system, charge separation  
127 occurs on a sub 100fs timescale, which was attributed to ballistic motion of the electrons  
128 through fullerene clusters.<sup>11</sup> Furthermore, using an EA signal, it has been shown that also  
129 polarons in a pBTTT:PCBM system can move on timescales <1ps between different phases  
130 of the BHJ, i.e. from a co-crystal region to domains of pure pBTTT.<sup>29</sup>

131  
132 But the EA signal also contains information about the molecules which are affected by the  
133 electric field of the separating e-h pair, as illustrated in the cartoon in Figure 1 (c).

134 Importantly, these molecules must lie at or near the interface between n- and p-type  
135 semiconductors. The observed EA signal resembles the first derivative of the absorption  
136 spectra of these molecules (see more details in the SI, Section S4), as reported in the  
137 literature on TA measurements<sup>11,29,30</sup> and steady-state EA experiments<sup>31</sup>. Integrating this over  
138 photon energy gives the ground state absorption spectra of these molecules. Thus, the EA  
139 signal could provide us a window on the energetic landscape experienced by charges as they  
140 move away from the interface. However, extracting pure EA signatures from pump-probe  
141 data is very difficult due to overlapping spectral signatures and energy relaxation (see  
142 Section S3.2).<sup>16</sup> Such signals also contain information from all the molecules influenced by  
143 the electric field, and this reduces the spatial resolution of the information we can obtain.

144

145 We present here a new pump-push-probe electroabsorption (PPP) technique, which uses a  
146 third ‘push’ pulse in order to obtain clean EA signatures on more localised areas. In this  
147 technique, the above-gap pump pulse creates a population of singlet excitons on the donor.  
148 After electron transfer, e-h pairs are created across the donor-acceptor interface. We follow  
149 this with a time-delayed ‘push’ pulse, at 2000nm (0.62eV), which is targeted in the low-  
150 energy PIA of the hole-polarons. Previously, it has been shown that this push pulse excites  
151 hole-polarons within their electronic manifold, briefly delocalising them. The holes will  
152 rapidly relax and localize on sub 200fs timescales, but some of them would have moved onto  
153 adjacent polymer chains.<sup>9</sup> Thus in our experiment, the push pulse acts as an optical method to  
154 move the hole-polaron. We note that the wavelength of the push pulse is chosen to be in a  
155 background free region where it does not overlap with absorptions from singlet or triplet  
156 exciton on the polymer, or charge transfer states, nor does it directly generate excitations on  
157 the polymer, as it is well below the bandgap. Importantly, as we report here, by moving the  
158 hole we change the electric field distribution caused by the e-h pair, as illustrated in Figure  
159 1 (d). The PPP signal thus contains a mix of GSB, PIA, SE and a modified EA signal. By

160 alternating the excitation sequence of the sample between pump-push and pump-only laser  
161 pulses, we are able to obtain a very clean subtraction of the pump-only signal from the pump-  
162 push signal. This leaves only the difference between the two EA signals (with and without  
163 push). As illustrated in Figure 1 (e), this EA signal reports only on the small subset of  
164 molecules brought into, or removed from, the influence of the electric field by the movement  
165 of the charge following the push pulse. As it is the hole polaron that is being pushed within  
166 the experiment, the change observed will come mostly from the movement of the hole within  
167 the polymer phase. This allows us to monitor just a small spatial volume around the hole-  
168 polaron, providing a nanoscale window into the energetic landscape near the interface and to  
169 trace it while it moves away from the interface towards the bulk. Thus, the experimental  
170 method presented here has analogies with super-resolution STED microscopy, in the use of a  
171 switching methodology (here by the use of the push pulse) to achieve a high spatial  
172 resolution.

173

174 For the sake of clarity, in the following text we focus our investigation on 4:1 and 1:4 for  
175 PCDTBT:mPCBM blends. The 1:4 blend provides best solar cell operation, with quantum  
176 yields for charge collection close to 100%<sup>14</sup> and the 4:1 blend provides a comparison as a  
177 system with efficient early time electron-hole pair generation but inefficient long-range  
178 charge separation. Also, both blends are on the extreme ends of the ordered and disordered  
179 scale. Data for others blends, which show similar trends to those discussed in the main text,  
180 are provided in the SI (see Section S3.3.1).

181

182 Figure 2(a) shows the map of PCDTBT:mono-PCBM (4:1) for excitation with both pump and  
183 push pulses. The sample is excited at 0 ps with a 500 nm pump pulse and pushed after 4.9 ps  
184 with a 2000 nm infrared pulse. Figure 2(b), shows the final map produced by the pump-push-  
185 probe experiment which gives only the differential signal induced by the push pulse. It can be



186 seen that the push pulse induces both a positive and a negative feature. We note that the zero-  
187 crossing, i.e. the transition point from positive to negative signals, in this map is at higher  
188 energies (roughly at 600 nm) compared to the normal pump-probe one (at around 650 nm),  
189 indicating that the signal is not related to an increased excited state population (see more  
190 details in the SI, Section S4).

191  
192 The main spectral component of the pump-push response, as revealed by a global analysis on  
193 the data, is shown in Figure 2(c). This feature is found to be well matched well with the  
194 steady-state EA spectrum, shown by the dotted line, which has been measured previously.<sup>11</sup>  
195 Thus, we find that the push pulse gives rise to an EA signal, as described above, which  
196 contains information on the molecules near the interface. We note that spectra taken from the  
197 raw data show the same trend (see Figure S3.5). However, the global analysis yields cleaner  
198 spectral signatures, more details on this can be found in the SI (Section S5).

199  
200 Figure 3(a) summarises the EA spectra obtained for the 4:1 and 1:4 for PCDTBT:mPCBM  
201 blends (data on other blends can be found in the SI, Figure S3.3). As described above, due to  
202 the derivative nature of the EA signal, integration yields the underlying absorption spectra of  
203 the molecules at and near the interface affected by the electric field of the e-h pair (as  
204 illustrated in Figure 1(e)). These interfacial absorption spectra are shown in Figure 3(b). We  
205 observe that for both blends the interfacial absorption is significantly red-shifted compared to  
206 the bulk of the polymer film (green dashed line, integration of CW EA of a  
207 PCDTBT:mPCBM film). This cannot be explained by the UV-Vis spectra of blends, that are  
208 only slightly red-shifted compared to the neat polymer (see Figure S1.2). Figure 3(c) shows  
209 the absorption spectra of the neat polymer film measured with photothermal deflection  
210 spectroscopy (PDS), which provides several orders of magnitude in detection sensitivity in  
211 absorption and is not distorted by reflection and scattering.<sup>32</sup> It can be seen that the interfacial

212 absorption measured via the PPP technique lies in the low-energy tail of the neat polymer  
213 film, whose absorption is two orders of magnitude below the absorption peak. This means  
214 that the polymer chains that make up the electronically active interfacial sites represent a very  
215 small fraction (<1%) of the total chains in the film. We consider that the very low energy of  
216 these electronically active interfacial sites must be related to highly planar and ordered  
217 polymer backbones, leading to larger wavefunction delocalisation and low bandgaps. This  
218 suggests that in all the blends studied here, the electronic dynamics at the interface are  
219 controlled by a very small fraction of sites (which are not representative of the bulk film)  
220 which are highly ordered, planar, and of lower energy than the bulk of the polymer film.

221

222 The widths of the absorption spectra are listed next to the legend in Figure 3(b) and  
223 correspond to the FWHM of a modified bi-Gaussian fit to the respective curve. The width of  
224 the obtained curves exhibits the same trend as the SAXS/WAXS results (see Section S2),  
225 which can be seen in the fullerene and polymer scattering peaks, indicating that order in one  
226 phase influences the other and therefore higher order of the fullerene leads to a more highly  
227 ordered polymer, i.e. increased fullerene content and better fullerene packing lead to  
228 increased order in the polymer phase near the interface. This ordering effect has been  
229 reported in the literature for the amorphous polymers PCDTBT and MDMO-PPV upon  
230 fullerene addition.<sup>19,22,33,34</sup>

231

232 We have also found similar trends of the EA feature using PCDTBT blended with a range of  
233 other fullerene derivatives: mPCBM, bPCBM, and tPCBM, as reported in the SI (Section  
234 S3.3.1). Here, for 1:1 blends the sample with tPCBM exhibits the strongest blue-shift and the  
235 highest FWHM value for the integrated EA spectrum, in good agreement with the largest  
236 disorder of PCDTBT:tPCBM. With decreasing disorder towards bPCBM and mPCBM, the  
237 spectra get further red-shifted and narrower. Furthermore, we find that pushing either the low

238 or higher-energy polaron PIA using 2000 nm or 1200 nm, respectively, both yields the same  
239 trend across blend disorder (see Figure S3.6). Using the 1200 nm push, blue and red-shifts  
240 get even more pronounced across the disorder series which could be related to a larger  
241 induced e-h distance and hence sampling a larger material volume.

242

243 The analysis above was performed for measurements in which the 2000 nm push pulse  
244 arrives 0.9 ps after the pump pulse. But by varying the time delay between pump and push  
245 pulses, we can monitor the differential EA signal as a function of time, as the e-h pairs  
246 separate and move away from the interface. This allows us to track the local environment  
247 experienced by the e-h pairs as a function of time.

248

249 Figure 4(a) shows integrated the EA spectra at different push times for the  
250 PCDTBT:mPCBM (4:1) blend. This ratio of polymer to fullerene gives rise to a blend in  
251 which fullerene are well dispersed within the polymer side chains and there are very few  
252 fullerene aggregates.<sup>20,35</sup> Though exciton dissociation is efficient in this blend, it does not  
253 give rise to long-range charge separation and shows low external quantum efficiencies (EQE)  
254 in OPV devices.<sup>11</sup> As shown in Figure 4(a), the spectra for the earliest time slices are the  
255 most red-shifted and blue-shift over time. This suggests that for the PCDTBT:mPCBM (4:1)  
256 blend, hole polarons are formed within lower-energy regions, where the polymer is relatively  
257 better ordered (leading to a red-shifted signal in Figure 4(a)), and then on picosecond  
258 timescales move into higher-energy more disordered regions, which more closely resemble  
259 the bulk of the polymer phase. Figure 4(c) shows this shifting of the peak as a function of  
260 time. This need to move from lower energy to higher energy areas, as charges move away  
261 from the interface, is clearly an energetically unfavourable configuration for long-range  
262 charge separation. This is consistent with the poor long-range charge separation and EQE and  
263 high geminate recombination in these blends.

264

265 In contrast, the PCDTBT:mPCBM (1:4) blend shows fullerene aggregates, gives rapid long-  
266 range charge separation and excellent EQE in devices.<sup>11</sup> As shown in Figure 4(b) the  
267 spectrum initially red-shifts strongly over the first 150 fs before blue-shifting over the next  
268 1 ps. The shifting of the peak position is shown in Figure 4(c). This suggests that charges are  
269 initially located in more disordered regions and rapidly move into regions with higher order  
270 within the first 150 fs. Such motion of charges from disordered to ordered regions is  
271 consistent with a model of the system in which charges are generated in a disordered mixed  
272 phase and then move into more ordered regions, lowering their energy while doing so.  
273 However, the timescale for this movement into ordered regions, 150 fs, suggests that charges  
274 are moving extremely rapidly at early times. Indeed, such fast timescales are inconsistent  
275 with incoherent charge hopping, but are consistent with previous observations of ballistic  
276 charge separation in the PCDTBT:mPCBM (1:4) blend, attributed to ballistic motion of  
277 electrons through fullerene clusters.<sup>11</sup> The results here suggest that the hole polaron also  
278 moves very rapidly on early time scales, exploring the local energetic landscape on 150 fs  
279 timescales and moving towards low energy, better ordered sites away from the interface. This  
280 early time motion allows the e-h pair to overcome the Coulomb barrier on sub 200 fs  
281 timescales with high efficiency. As a result, this blend ratio shows very little geminate  
282 recombination.<sup>9,16</sup>

283

284 At later times, the charges then slowly move back into more disordered polymer regions on  
285 ps timescales, as they move away from the interface and into the bulk of the polymer.  
286 However, since e-h separation beyond the Coulomb capture range (considered to be 5 nm<sup>11</sup>)  
287 was achieved at early times, this later time, energetically unfavourable motion does not seem  
288 to hinder device performance. We also note, that having interfacial sites that are higher  
289 energy than neighbouring sites adjacent to the interface would also prevent charges from

290 moving towards the interface at longer timescales, acting as a barrier to longer time non-  
291 geminate recombination.

292

293 Our results reveal that, very surprisingly, in polymer-fullerene blends the electronically active  
294 interfacial sites lie in the low-energy tail of the neat polymer film, forming a very small  
295 subset of the total chains in the film. These low energy sites are most likely highly planar and  
296 ordered polymer chains, which enables larger wavefunction delocalisation and low bandgaps.  
297 We note that these sites are different from CT states which exhibit transitions at much lower  
298 energies of around 1.46 eV (see Figure S1.1).<sup>17</sup> In unoptimised 4:1 polymer:fullerene blends,  
299 charges are formed at the lowest energy sites, and moving away from the interface entails an  
300 energetic penalty, leading to low EQEs and high geminate recombination. For the optimised  
301 1:4 polymer:fullerene blend the interfacial energetics drive a very rapid, sub 150fs, motion of  
302 hole polarons away from the higher energy interfacial sites to low energy more highly  
303 ordered sites. This rapid motion helps to overcome the Coulomb interaction and is consistent  
304 with early time ballistic charge transport. Thus, the energetic structure of the interface and the  
305 regions adjacent to it, are key to understanding both the poor EQEs of the 4:1 polymer-  
306 fullerene blend as well as the very high EQEs in the 1:4 blend. This new all-optical method  
307 developed here provides a unique window on the molecular ordering and energetic landscape  
308 and electronic dynamics of interfacial sites. The technique is a straightforward modification  
309 of the widely used technique of optical pump-probe spectroscopy and can readily be extended  
310 to other disordered, buried semiconductor interfaces across which electron-hole pairs can be  
311 generated. This may include interfaces such as organic/metal-oxides<sup>36</sup>, organic/perovskite<sup>37</sup>,  
312 organic/colloidal quantum dots (CQD)<sup>38,39</sup>, CQD/CQD heterojunctions<sup>40</sup>, and CQD/metal-  
313 oxide junctions<sup>40</sup>.

314

315 **Methods:**

316 **Sample preparation:**

317 PCDTBT was purchased from 1-material, PCBM, bis-PCBM, tris-PCBM were purchased  
318 from Solenne BV. All materials were used as received.

319 Polymer:fullerene blends were spun from ortho-dichlorobenzene with 10 mg/ml for 4:1, and  
320 1:1 blends (polymer:fullerene mass ratio) and 15 mg/ml for 1:4 blends, respectively. Films  
321 were prepared on ultrathin glass substrates (130  $\mu\text{m}$ ) which were cleaned by sonication in  
322 acetone and isopropyl alcohol and exposure to  $\text{O}_2$  plasma for 10 min each. Substrates were  
323 subsequently brought in an oxygen and water free glovebox ( $\text{O}_2 < 5 \text{ ppm}$ ,  $\text{H}_2\text{O} < 1 \text{ ppm}$ ) and  
324 spun at 1500 RPM for 120 s. Films were encapsulated in the glovebox using microscope  
325 cover slides as spacer between film and second ultrathin cover glass, sealing the edges with  
326 epoxy resin.

327

328 **Ultrafast Transient Absorption Spectroscopy (TA):**

329 Transient Absorption spectra were acquired using a 1 kHz regenerative Ti:Sapphire amplifier  
330 (Solstice, Spectra-Physics), seeding two homebuilt broadband non-collinear optical  
331 parametric amplifiers (NOPAs). One NOPA was used as a broadband visible probe while the  
332 other NOPA was used as the pump source, tuned to 500 nm pulses with  $9 \mu\text{J}/\text{cm}^2$  (1200 nm  
333 push) and  $40 \mu\text{J}/\text{cm}^2$  (2000 nm push) pulse energy, respectively, after compression using a  
334 pair of dielectric chirped mirrors (Layertec 109811) and chopped at 500 Hz. The probe light  
335 was split into two separate beams, one probe and one reference beam. Both got dispersed  
336 with a grating spectrometer (Shamrock SR-303i, Andor Technology) and measured  
337 simultaneously with a CCD detector array each (Entwicklungsbüro Stresing). Here, the  
338 reference is not subject to the pump beam and is therefore used to correct for shot-to-shot  
339 fluctuations in the system.

340 For pump-push-probe measurements, we used the TA setup described above and a  
341 commercial OPA (TOPAS, Light-Conversion) to create the infrared push pulse of 2000 nm at  
342 25 mJ/cm<sup>2</sup> and 1200 nm at 3 mJ/cm<sup>2</sup> for the respective experiments, chopped at 250 Hz. The  
343 wavelengths of the push are tuned to the low energy edge of the respective polaron PIA  
344 bands (Figure S3.1). The high fluence of the push pulse is needed due to the low absorption  
345 cross-section of the excited states in this spectral region. Mathematical processing of the  
346 acquired data is described in Section S3.3.3 and more details on the global analysis can be  
347 found in Section S5. Each of the presented data curves is the result of an average over 8  
348 individual global analysis fits per dataset.

349

#### 350 **Wide / Small Angle X-ray Scattering (WAXS / SAXS):**

351 The WAXS/SAXS characterization has been performed according to previous works (ref.41)  
352 and reproduced here for completeness: Combined SAXS and WAXS measurements of the  
353 bulk material were carried out at the SAXS beamline of the Australian Synchrotron using a  
354 Pilatus 1M and a Pilatus 200k detector. The beam energy and detector distances were chosen  
355 in such a way, that there was a small overlap between the SAXS and WAXS signal, so that  
356 the resulting curves could be stitched together at  $q = 0.73 \text{ \AA}^{-1}$ .

357

#### 358 **Photothermal Deflection Spectroscopy (PDS):**

359 The PDS sample was prepared by spin-coating PCDTBT from 10 mg/ml solution in ortho-  
360 dichlorobenzene on water free quartz substrates (Spectrosil).

361 The experiment has been carried out as reported in previous works (ref.42) and is reproduced  
362 here for completeness: PDS is a scatter-free surface sensitive absorption measurement  
363 capable of measuring 5-6 orders of magnitude weaker absorbance than the band edge  
364 absorption.

365 For the measurements, a monochromatic pump light beam is shined on the sample which on  
366 absorption produces a thermal gradient near the sample surface via non-radiative relaxation  
367 induced heating. This results in a refractive index gradient in the area surrounding the sample  
368 surface. This refractive index gradient is further enhanced by immersing the sample in an  
369 inert liquid FC-72 Fluorinert® (3M Company) which has a high refractive index change per  
370 unit change in temperature. A fixed wavelength CW laser probe beam is passed through this  
371 refractive index gradient producing a deflection proportional to the absorbed light at that  
372 particular wavelength, which is detected by a photo-diode and lock-in amplifier combination.  
373 Scanning through different wavelengths gives us the complete absorption spectra. Because  
374 this technique makes use of the non-radiative relaxation processes in the sample, makes it  
375 immune to optical effects like interference and scattering.

376

#### 377 **Data availability:**

378 The datasets generated during and/or analysed during the current study are available in the  
379 University of Cambridge data repository at <https://doi.org/10.17863/CAM.6924>.

380

#### 381 **Acknowledgements:**

382 We would like to thank S. Gélinas, N. Paul, and F. Deschler for fruitful discussions. This  
383 work was supported by the Engineering and Physical Sciences Research Council (EPSRC)  
384 and the Winton Programme for the Physics of Sustainability. A.C.J. thanks the University of  
385 Cambridge for funding (CHESS). Synchrotron measurements were undertaken on the SAXS  
386 beamline at the Australian Synchrotron, Victoria, Australia and we acknowledge the help of  
387 Niraj Lal with the measurements. S.H. thanks the framework project Soltech for funding.

388

#### 389 **Author Contributions:**



390 A.C.J. performed the pump-push-probe measurements, M.L.B. and S.H. performed the  
391 SAXS/WAXS experiments, A.S. conducted the PDS measurement. A.C.J., M.L.B., A.S., and  
392 S.H. analysed the data. A.R. and R.H.F. supervised the work. A.C.J., A.R., and R.H.F. wrote  
393 the manuscript. All authors commented on the manuscript.

394

395 **References:**

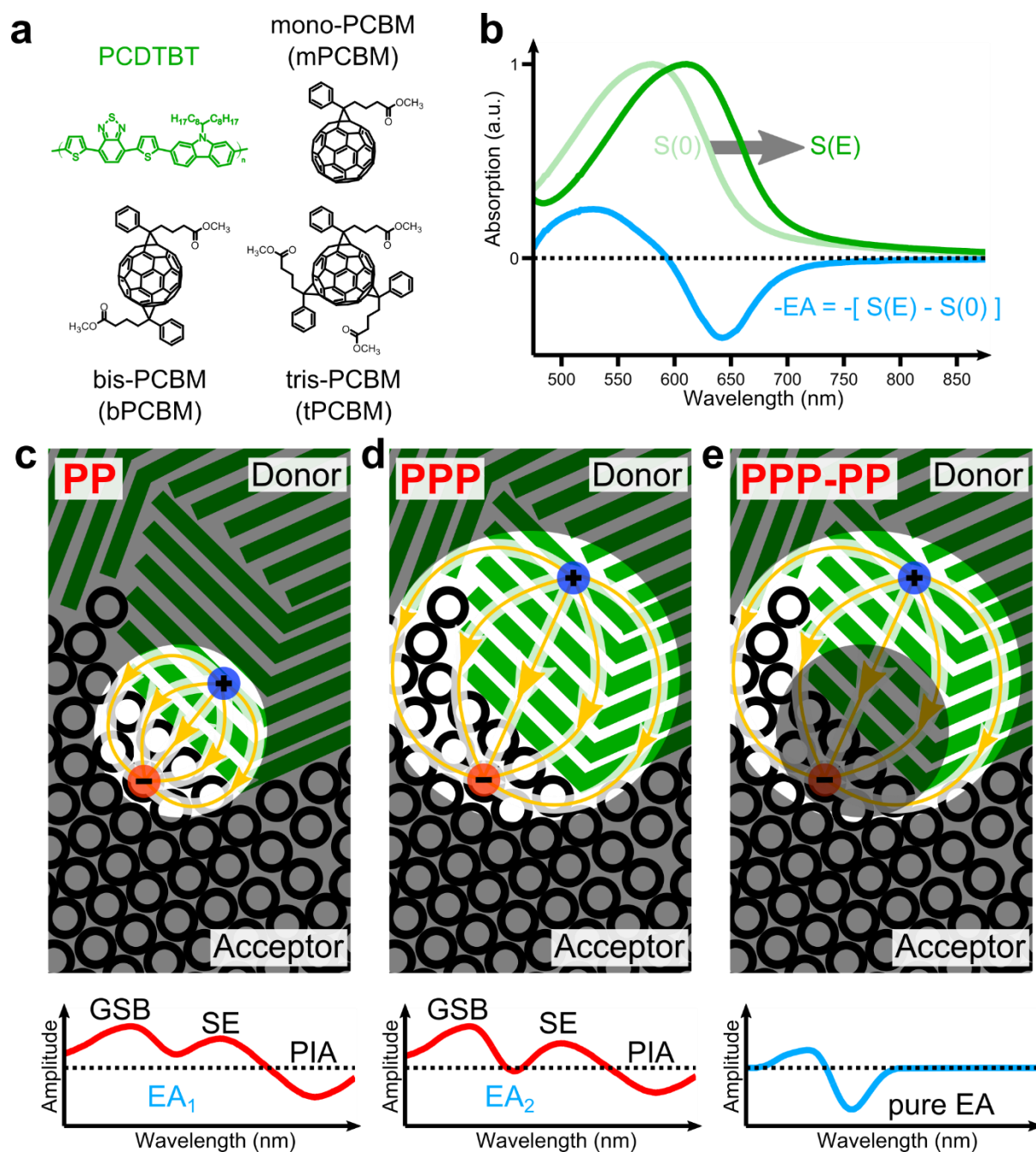
- 396 1. Agostini, G. & Lamberti, C. *Characterization of Semiconductor Heterostructures and*  
397 *Nanostructures (Second Edition)*. (2013).
- 398 2. Geiger, F. M. Second Harmonic Generation, Sum Frequency Generation, and  $\chi(3)$ :  
399 Dissecting Environmental Interfaces with a Nonlinear Optical Swiss Army Knife.  
400 *Annu. Rev. Phys. Chem.* **60**, 61–83 (2009).
- 401 3. Tang, C. W. Two-layer organic photovoltaic cell. *Appl. Phys. Lett.* **48**, 183–185  
402 (1986).
- 403 4. Halls, J. J. M. *et al.* Efficient photodiodes from interpenetrating polymer networks.  
404 *Nature* **376**, 498–500 (1995).
- 405 5. Yu, G. & Heeger, A. J. Charge separation and photovoltaic conversion in polymer  
406 composites with internal donor/acceptor heterojunctions. *J. Appl. Phys.* **78**, 4510–4515  
407 (1995).
- 408 6. He, X. *et al.* Formation of Nanopatterned Polymer Blends in Photovoltaic Devices.  
409 *Nano Lett.* **10**, 1302–7 (2010).
- 410 7. He, X. *et al.* Formation of Well-Ordered Heterojunctions in Polymer:PCBM  
411 Photovoltaic Devices. *Adv. Funct. Mater.* **21**, 139–146 (2011).
- 412 8. Pfadler, T. *et al.* Influence of Interfacial Area on Exciton Separation and Polaron  
413 Recombination in Nanostructured Bilayer All-Polymer Solar Cells. *ACS Nano* **8**,  
414 12397–12409 (2014).
- 415 9. Bakulin, A. A. *et al.* The Role of Driving Energy and Delocalized States for Charge  
416 Separation in Organic Semiconductors. *Science* **335**, 1340–1344 (2012).
- 417 10. Rao, A. *et al.* The role of spin in the kinetic control of recombination in organic  
418 photovoltaics. *Nature* 6–11 (2013). doi:10.1038/nature12339
- 419 11. Gelinas, S. *et al.* Ultrafast Long-Range Charge Separation in Organic Semiconductor  
420 Photovoltaic Diodes. *Science* **343**, 512–516 (2014).

- 421 12. Kouijzer, S. *et al.* Predicting Morphologies of Solution Processed Polymer:Fullerene  
422 Blends. *J. Am. Chem. Soc.* **135**, 12057–12067 (2013).
- 423 13. Huang, Y., Kramer, E. J., Heeger, A. J. & Bazan, G. C. Bulk Heterojunction Solar  
424 Cells: Morphology and Performance Relationships. *Chem. Rev.* **114**, 7006–7043  
425 (2014).
- 426 14. Park, S. H. *et al.* Bulk heterojunction solar cells with internal quantum efficiency  
427 approaching 100%. *Nat. Photonics* **3**, 297–302 (2009).
- 428 15. Banerji, N., Cowan, S., Leclerc, M., Vauthey, E. & Heeger, A. J. Exciton Formation,  
429 Relaxation, and Decay in PCDTBT. *J. Am. Chem. Soc.* 17459–17470 (2010).  
430 doi:10.1021/ja105290e
- 431 16. Etzold, F. *et al.* Ultrafast Exciton Dissociation Followed by Nongeminate Charge  
432 Recombination in PCDTBT:PCBM Photovoltaic Blends. *J. Am. Chem. Soc.* **133**,  
433 9469–79 (2011).
- 434 17. Provencher, F. *et al.* Slow geminate-charge-pair recombination dynamics at polymer:  
435 Fullerene heterojunctions in efficient organic solar cells. *J. Polym. Sci. Part B Polym.*  
436 *Phys.* **50**, 1395–1404 (2012).
- 437 18. Provencher, F. *et al.* Direct observation of ultrafast long-range charge separation at  
438 polymer-fullerene heterojunctions. *Nat. Commun.* **5**, 4288 (2014).
- 439 19. Beiley, Z. M. *et al.* Morphology-Dependent Trap Formation in High Performance  
440 Polymer Bulk Heterojunction Solar Cells. *Adv. Energy Mater.* **1**, 954–962 (2011).
- 441 20. Cates Miller, N. *et al.* Molecular Packing and Solar Cell Performance in Blends of  
442 Polymers with a Bisadduct Fullerene. *Nano Lett.* **12**, 1566–70 (2012).
- 443 21. Cates Miller, N. *et al.* Factors Governing Intercalation of Fullerenes and Other Small  
444 Molecules Between the Side Chains of Semiconducting Polymers Used in Solar Cells.  
445 *Adv. Energy Mater.* **2**, 1208–1217 (2012).
- 446 22. Cates, N. C., Gysel, R., Dahl, J. E. P., Sellinger, A. & McGehee, M. D. Effects of

- 447 Intercalation on the Hole Mobility of Amorphous Semiconducting Polymer Blends.  
448 *Chem. Mater.* **22**, 3543–3548 (2010).
- 449 23. Jakowetz, A. C. *et al.* What Controls the Rate of Ultrafast Charge Transfer and Charge  
450 Separation Efficiency in Organic Photovoltaic Blends. *J. Am. Chem. Soc.* **138**, 11672–  
451 11679 (2016).
- 452 24. Savoie, B. M. *et al.* Mesoscale molecular network formation in amorphous organic  
453 materials. *Proc. Natl. Acad. Sci. U. S. A.* **111**, 10055–10060 (2014).
- 454 25. Savoie, B. M., Jackson, N. E., Chen, L. X., Marks, T. J. & Ratner, M. A. Mesoscopic  
455 features of charge generation in organic semiconductors. *Acc. Chem. Res.* **47**, 3385–  
456 3394 (2014).
- 457 26. Cabanillas-Gonzalez, J., Grancini, G. & Lanzani, G. Pump-probe spectroscopy in  
458 organic semiconductors: monitoring fundamental processes of relevance in  
459 optoelectronics. *Adv. Mater.* **23**, 5468–85 (2011).
- 460 27. Sebastian, L., Weiser, G. & Bässler, H. Charge transfer transitions in solid tetracene  
461 and pentacene studied by electroabsorption. *Chem. Phys.* **61**, 125–135 (1981).
- 462 28. Yang, Y. *et al.* Semiconductor interfacial carrier dynamics via photoinduced electric  
463 fields. *Science* **350**, 1061 LP-1065 (2015).
- 464 29. Scarongella, M. *et al.* A Close Look at Charge Generation in Polymer:Fullerene  
465 Blends with Microstructure Control. *J. Am. Chem. Soc.* **137**, 2908–2918 (2015).
- 466 30. De Jonghe-Risse, J. *et al.* Using the Stark effect to understand charge generation in  
467 organic solar cells. in *Proc. of SPIE* (eds. Hayes, S. C. & Bittner, E. R.) **9549**, 95490J  
468 (2015).
- 469 31. Tsutsumi, J., Yamada, T. & Hasegawa, T. Electroabsorption Study of Charge-Transfer  
470 Excited State in Donor-Acceptor-Type Polymer. *Trans. Mater. Res. Soc. Japan* **39**,  
471 217–219 (2014).
- 472 32. Sadhanala, A. *et al.* Preparation of Single-Phase Films of  $\text{CH}_3\text{NH}_3 \text{Pb}(\text{I}_{1-x}\text{Br}_x)_3$  with

- 473 Sharp Optical Band Edges. *J. Phys. Chem. Lett.* **5**, 2501–2505 (2014).
- 474 33. Melzer, C., Koop, E. J., Mihailetschi, V. D. & Blom, P. W. M. Hole Transport in  
475 Poly(phenylene vinylene)/Methanofullerene Bulk-Heterojunction Solar Cells. *Adv.*  
476 *Funct. Mater.* **14**, 865–870 (2004).
- 477 34. Tuladhar, S. M. *et al.* Ambipolar Charge Transport in Films of Methanofullerene and  
478 Poly(phenylenevinylene)/Methanofullerene Blends. *Adv. Funct. Mater.* **15**, 1171–1182  
479 (2005).
- 480 35. Mayer, A. C. *et al.* Bimolecular Crystals of Fullerenes in Conjugated Polymers and the  
481 Implications of Molecular Mixing for Solar Cells. *Adv. Funct. Mater.* **19**, 1173–1179  
482 (2009).
- 483 36. Greiner, M. T. & Lu, Z.-H. Thin-film metal oxides in organic semiconductor devices:  
484 their electronic structures, work functions and interfaces. *NPG Asia Mater* **5**, e55  
485 (2013).
- 486 37. Stranks, S. D. & Snaith, H. J. Metal-halide perovskites for photovoltaic and light-  
487 emitting devices. *Nat Nano* **10**, 391–402 (2015).
- 488 38. Morgenstern, F. S. F. *et al.* Ultrafast Charge- and Energy-Transfer Dynamics in  
489 Conjugated Polymer: Cadmium Selenide Nanocrystal Blends. *ACS Nano* **8**, 1647–  
490 1654 (2014).
- 491 39. Böhm, M. L. *et al.* The Influence of Nanocrystal Aggregates on Photovoltaic  
492 Performance in Nanocrystal-Polymer Bulk Heterojunction Solar Cells. *Adv. Energy*  
493 *Mater.* **4**, (2014).
- 494 40. Carey, G. H. *et al.* Colloidal Quantum Dot Solar Cells. *Chem. Rev.* **115**, 12732–12763  
495 (2015).
- 496 41. Mueller, C. J., Singh, C. R., Fried, M., Huettner, S. & Thelakkat, M. High Bulk  
497 Electron Mobility Diketopyrrolopyrrole Copolymers with Perfluorothiophene. *Adv.*  
498 *Funct. Mater.* **25**, 2725–2736 (2015).

499 42. Price, M. B. *et al.* Hot-carrier cooling and photoinduced refractive index changes in  
500 organic–inorganic lead halide perovskites. *Nat. Commun.* **6**, 8420 (2015).  
501



503

504 **Figure 1:** Origin of the electroabsorption signal in pump-probe and pump-push-probe

505 measurements. (a) Chemical structures of PCDTBT and PCBM fullerene acceptors. (b)

506 Schematic origin of the spectral electroabsorption (EA) features due to a Stark shift of energy

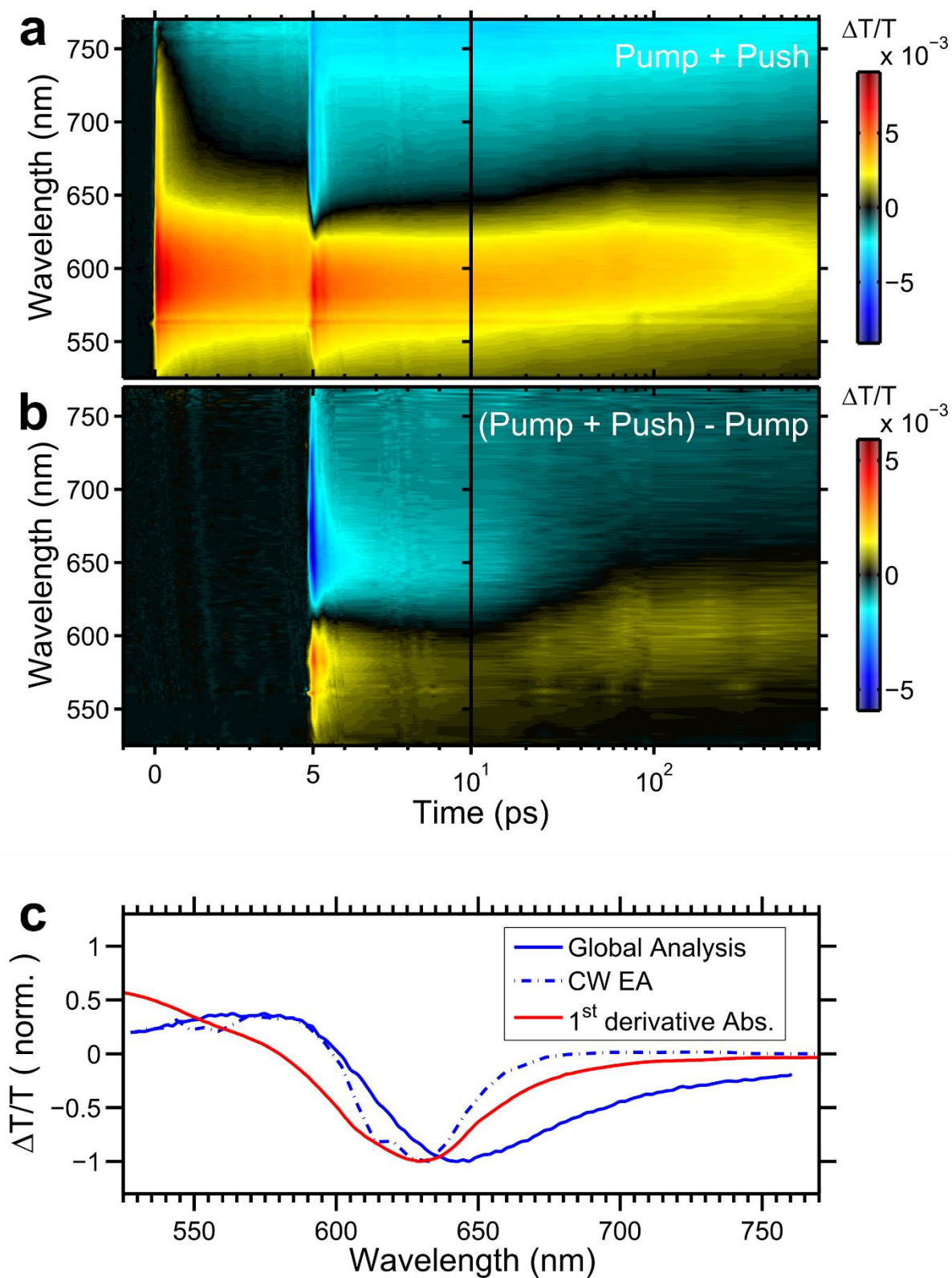
507 levels of the ground state absorption  $S(0)$  in the presence of an electric field  $S(E)$ . The

508 electric field shift is exaggerated to highlight the resulting spectrum, which is flipped in sign

509 for better comparison with the feature observed in transient absorption. (c) States probed by

510 *pump-probe (PP) and a qualitative spectrum composed of the different components. Signals*  
511 *like the ground-state bleach (GSB), stimulated emission (SE) and photo-induced absorption*  
512 *(PIA) are specific to the site occupied by the charges. In contrast, the EA contains*  
513 *information from molecules in the volume influenced by the electric field, as shown by the*  
514 *brightened region. Only few electric field lines are shown and the extension to the ‘outside’*  
515 *of the electron hole pair is omitted for simplicity reasons. The dotted line in the signal sketch*  
516 *represents the zero value of the signal amplitude. (d) States probed by pump-push-probe*  
517 *(PPP) and a corresponding sketch of a qualitative spectrum. The push pulse moves the hole*  
518 *away from its original position. The electron-hole separation is increased and the electric*  
519 *field changed. Therefore, the EA signal is changed as indicated by the enlarged brightened*  
520 *area, while the site specific signals, such as GSB, SE and PIA are not changed as they still*  
521 *arise from the same electronic species (charges). (e) Subtraction of PP from the PPP, yields*  
522 *a small spatial area (indicated by the remaining brightened area) from which a pure EA*  
523 *signal of the area near the interface of the bulk-heterojunction can be retrieved.*



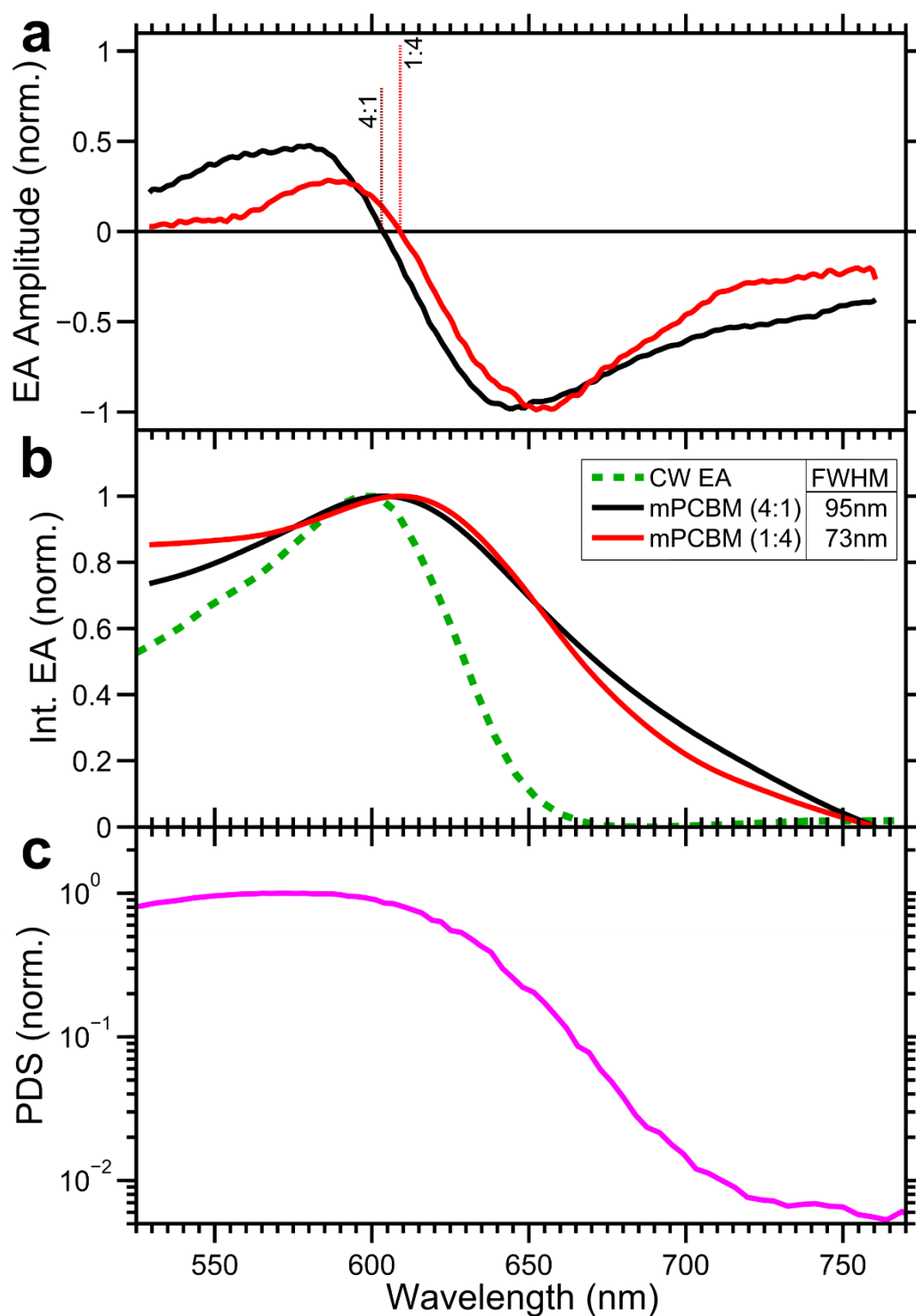


525

526 **Figure 2:** Pump-push-probe data for PCDTBT:mono-PCBM (4:1) with 500 nm pump and

527 2000 nm push pulses arriving after 4.9 ps delay. (a) Full TA map with pump and push pulses

528 *present and (b) the differential TA map between pump-push-probe and pump-probe revealing*  
529 *the influence of the push pulse only. We note that the direct sequence of pulses allows us to*  
530 *obtain data of high accuracy by purely subtracting the pump-probe dataset, as can be seen*  
531 *from the zero signal region for times smaller than 4.9 ps. (c) The main spectral component of*  
532 *a global analysis of this differential TA map, which is found to match the electroabsorption*  
533 *(EA) spectrum, alongside a reference spectrum from steady-state EA measurement (CW EA)*  
534 *and the first derivative of the absorption spectrum (red).*



536

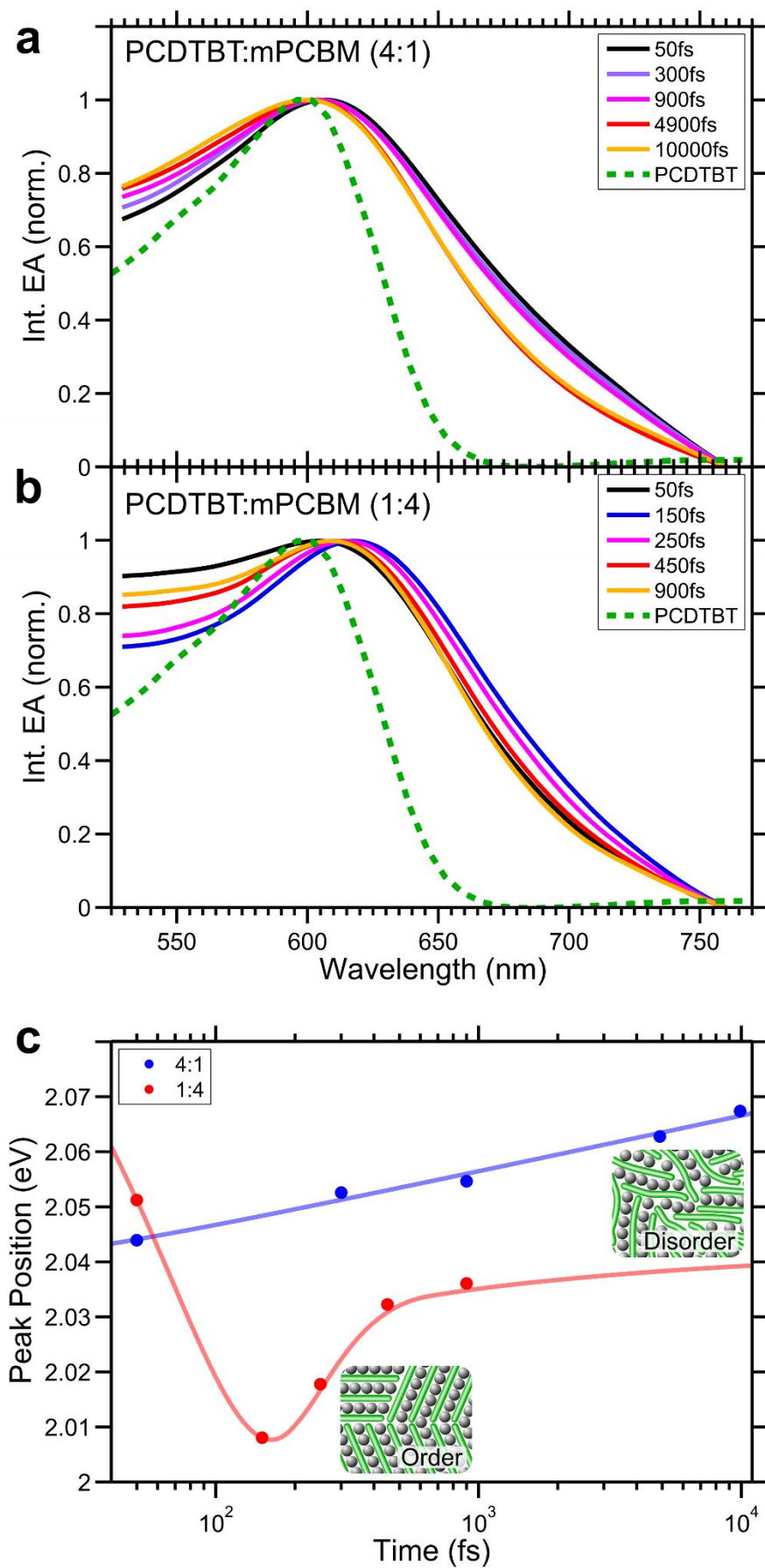
537 **Figure 3:** Pump-push-probe measurements and resulting EA spectra on PCDTBT:mPCBM

538 4:1 (black) and 1:4 (red) blends. (a) EA spectra obtained from global analysis on the

539 difference TA map between pump-push-probe and pump-probe datasets with the push pulse

540 arriving 0.9 ps after initial excitation. These differential TA maps represent the pure impact

541 *of the push pulse. With the push not being absorbed by the ground state, the EA response*  
542 *arises only from moving hole-polarons via the push pulse. (b) Integrated EA spectra from (a)*  
543 *including the integrated CW EA signal (green dashed line, measured on a diode under*  
544 *applied electrical field), which is indicative of the steady state absorption of the film. The*  
545 *column next to the legend shows the FWHM of a bi-Gaussian fit to the respective curve. (c)*  
546 *PDS spectra of a thin film of neat PDCTBT, giving insights into low energy tail states (note*  
547 *the log scale).*



550 **Figure 4:** Spectral signatures of charges moving through different material regions after the  
551 initial charge transfer step. **(a)** Integrated EA spectra obtained from global analysis on the  
552 differential TA map between pump-push-probe (PPP) and pump-probe (PP) datasets of the  
553 PCDTBT:mPCBM (4:1) blend. Spectra were recorded at different delays between pump and  
554 push pulses ranging from 50 fs to 10 ps. The integrated CW EA signal (green dashed line) is  
555 included to indicate the steady state absorption of the film. **(b)** Integrated EA spectra from  
556 global analysis on the PPP-PP differential map of the PCDTBT:mPCBM (1:4) composition.  
557 Here, time delays between pump and push pulses were varied between 50 fs and around 1 ps  
558 with more steps at earlier times due to the faster charge generation timescale. The integrated  
559 CW EA signal (green dashed line) is included to indicate the steady state absorption of the  
560 film. **(c)** Peak positions of integrated EA signals of 4:1 (blue symbols) and 1:4 (red symbols)  
561 PCDTBT:mPCBM blends with regard to the respective pump-push delays. While holes in the  
562 4:1 blend slowly migrate to more disordered regions, in the 1:4 blends, they move into more  
563 ordered regions on 150fs timescales, followed by a slower movement into slightly more  
564 disordered regions. The solid lines are guides to the eye and the cartoons are show planar  
565 and disordered polymer chains. We note that they are not meant to represent the real  
566 morphology.